Zhang, K., Hatano, T., Herrmann, G., Antognozzi, M., Edwards, C., Burgess, S., ... Miles, M. (2018). Enhancing fixed-point control robustness for experimental non-contact scans with the Transverse-dynamic Force Microscope. In *American Control Conference 2018 (ACC 2018)* Institute of Electrical and Electronics Engineers (IEEE).

Peer reviewed version

Enhancing fixed-point control robustness for experimental non-contact scans with the Transverse-dynamic Force Microscope*

K. Zhang[1], T. Hatano[1], G. Herrmann[1], M. Antognozzi[2],
C. Edwards[3], S.C. Burgess[1], T. Nguyen[4], and M. Miles[2]

***Abstract*— The Transverse Dynamic Force Microscope (TDFM) is unique as it uses a vertical cantilever, and genuinely permits scans without physical interaction with a specimen. Recently, we suggested a simple control scheme for true non-contact scans using the TDFM. This control scheme implemented in FPGA-systems (Field-Programmable Gate Arrays) was developed for a non-contact control task at specific points above a given specimen, but dynamic specimen placement requirements in the horizontal plane through an x-y stage were neglected. Considering the large range of the specimen, a practical approach has been developed which reconfigures the fixed-point-arithmetic control implementation and permits a dynamic scan in true non-contact mode. For this, an off-line numerical optimization has been developed which establishes the most suitable fixed-point ranges of the control algorithm, avoiding algorithm overflow. This creates an implementation robust to plant and sensor non-linearities and dynamic changes during non-contact scans. Experimental non-contact scanning results, for nano-spheres in water, demonstrate the imaging capacity of the TDFM.**

I. INTRODUCTION

Shear force microscopy (SFM) works with a vertically mounted cantilever [1], [2], [3], [4], [5], [6], [7], in contrast to most other atomic force microscope (AFM) setups (e.g. [8], [9]). The basic principle is to excite the vertical cantilever, usually at one of its modal frequencies. Once brought closer to the specimen, the cantilever oscillation characteristics, like phase and amplitude, change with respect to the increasing shear force due to the interaction with the specimen.

In early SFM-research, focus has been given to the mechanisms for cantilever excitation and cantilever tip motion detection. The use of a tuning fork for excitation was a successful passive actuation device, but it had a low resonance frequency of 33kHz and subsequently slow detection and scanning speeds [5]. Ultrasound [6] (with sensitivity around 33 kHz) or laser interferometry [10] (tungsten cantilever tip diameter of 120 μm) for tip detection was considered but did not permit further miniaturization of the cantilever, again limiting bandwidth. At Bristol, research on SFMs has been ongoing for more than 17 years: in particular the development of a highly sensitive evanescent field detection mechanism allowing for high excitation frequencies and extreme cantilever miniaturization. This sensing scheme allowed extreme low dynamic force detection and soft specimen scans [10], [11]. This strand of SFMs is in fact unique to Bristol [2], [3], [4]; hence the use of the specific term, TDFM. The other advantage of Bristol's TDFM is its potential to achieve high speed non-contact scanning. The cantilevers have a resonant frequency range from $166kHz$ to $1.66MHz$, which in principle allows faster scanning than other high-speed AFMs [8]. The TDFM uses two measurements from a scattered evanescent field [2] below the specimen: the overall light strength, and the relative position of the oscillating cantilever [12]. Within a small ordered water layer of about $20nm$, the cantilever oscillation amplitude decreases in a monotonic manner when approaching the specimen. This allows non-contact scans.

Over the last decade, the TDFM has been used as an atomic force detection tool [13] and a scanning tool [4]. In a previous fast high-precision application of [4], the TDFM employs a traditional PI controller to keep a constant height from the tip to the glass sample-holder using an optical feedback strategy. As a result, it has (mainly) sensitivity to the top of the samples in the shear-force interacting range. The part of the topography where the distance from the cantilever to the sample-substrate exceeds the interacting range, cannot be imaged. In [12], we developed a control scheme which exploits the cantilever oscillation amplitude for closed-loop control. This keeps a constant distance between the oscillating cantilever and the sample-substrate. However, the control was only validated for a single position above the specimen. The FPGA-implementation at that time was still limited – often resulting in numerical overflows due to the dynamic scanning action. Moreover, topography-data streaming at a large rate had to be ensured. However, there is strong benefit from using a bespoke FPGA-based control implementation (in contrast to for instance fast analogue circuits [8] or a phase-locked loop based controller (PLL) [5], [6]); this introduces greater flexibility for controller change and (in particular in relation to PLLs) permits higher bandwidth control loops and potentially faster scanning.

This paper focuses therefore on a practical solution to implement fixed-point-arithmetic based digital control for complete non-contact mode scans using TDFM , in contrast to the single point result of [12]. Digital control of the TDFM has been developed using FPGA technology, which is a common tool in the AFM control area (e.g. [14], [15], [16], [17] etc.). The literature, e.g. [14], on implementing fixed-point-arithmetic digital controllers with FPGAs in this context is rather limited and not very systematic. Hence, this paper suggests a simulation scheme to verify the possibility of FPGA based digital control design to improve the efficiency of practical control development. An optimiza-

*This work was funded by EPSRC grants EP/I034882/1 & EP/I034831/1

[1]Department of Mechanical Engineering, Univ. of Bristol, University Walk, Bristol, BS8 1TR, UK G.Herrmann@bris.ac.uk

[2]Centre for Nanoscience and Quantum Information, Univ. of Bristol, UK

[3]College of Engineering, Mathematics and Physical Sciences, Univ. of Exeter, EX4 4QF, UK

[4]Faculty of Electrical & Electronics Engineering, Ton Duc Thang Univ., Ho Chi Minh City, Vietnam

tion using simulation is proposed as a guidance tool for practical implementation. Based on the non-contact sensing mechanism in [12], the implemented digital control solution provides the ability to realize practically an analysis of plant dynamics (in closed-loop), high order controllers, and non-contact scans.

II. THE TDFM SYSTEM AND FEEDBACK LOOP DESIGN

A. The TDFM System

While the first principles of the TDFM were developed more than 25 years ago [1], the essential sensing mechanism for small, soft, but high frequency cantilevers was invented at the University of Bristol [2], [4]. The TDFM consists of three core components as shown in Figure 1: a) a TDFM-head at a fixed position (including ①, ②, ③, ④) to provide the vertically oriented cantilever motion along the z-axis and horizontal excitation along y-axis (the slow-raster-actuation axis in raster scans); b) an x-y horizontal stage (shown as ⑨ in Figure 1) to hold the sample and provide horizontal in-plane motion in the x-y directions; c) an optical system (simplified as ⑧, ⑩, ⑪ in Figure 1) to provide the evanescent field for measurement proposes [2].

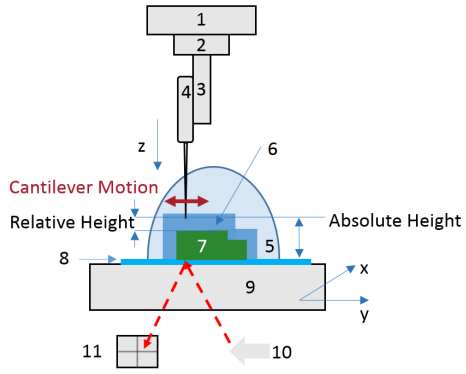

Fig. 1: Schematic of the TDFM. The numbered components are: 1) Vertical coarse piezo-actuator; 2) Vertical fine piezo-actuator; 3) Horizontal dither piezo-actuator; 4) Vertically oriented cantilever; 5) Liquid environment; 6) Ordered water layer covering the sample-substrate; 7) Scanning specimen; 8) Glass slide to hold the sample; 9) Horizontal stage; 10) Inlet laser to generate an evanescent field. 11) Photo-detector.

The cantilever is extended from a super-low-stress silicon nitride chip (see Figure 1) (Nu Nano Ltd., 2017, NuVOC Select 200). The ultrasoft cantilever is selected to be $40\mu m$ in length, $1\mu m$ in width, and $200nm$ in thickness with a spring-constant of $0.006563N/m$. The chip is then attached to a holder at the end of the TDFM-head. To realize the sensing mechanism, three piezo-actuators are used on the TDFM-head: a) a dither piezo-actuator (ceramic plate) (Physik Instrumente (PI) GmbH, 2016, www.pi.ws) to horizontally excite the cantilever at or close to the cantilever's resonant frequency; b) a coarse piezo-actuator (P-885.51) (PI) to provide the cantilever a large constant offset to position it within the evanescent field. Such a positioning action is not easy to carry out via closed-loop control as the sensitivity of the cantilever detection is highly nonlinear and also strongly distance limited; c) a fine piezo-actuator (PL055.30) (PI) to drive the cantilever in the vertical direction (z-axis) for feedback control when scanning the specimen.

The optical system developed in [2] provides two distance measurements (see Figure 1): a) relative height: the distance from the cantilever to the sample-substrate. (In particular, the oscillation amplitude reduces as the shear force grows with increasing penetration into the ordered water layer.); b) absolute height: incremental changes in distance of the cantilever to the quartz sample holder cause the total light intensity of the tuned evanescent field to decrease.

For non-contact scanning with the TDFM, a constant relative height between the oscillating cantilever and the sample-substrate has to be maintained while taking the absolute height to image the topography. Thus, the objective is to control the oscillating amplitude by driving the fine piezo-actuator along the vertical z-axis: i.e. the relative height is controlled to track the changing sample-substrate topography.

B. Vertical Non-contact Feedback Control Design

The control system is realized by two digital functional components: the relative height sensing mechanism and the feedback control.

The relative height sensing mechanism is designed to sense the dynamic change in the oscillation amplitude of the cantilever. This algorithm runs as an isolated functional component, which employs a National-Instrument (NI)-7962R FPGA board (National Instruments Co., 2017, www.ni.com). In a water-based environment, the cantilever oscillation at $350kHz$ measured by the photo-detector is first amplified by a pre-amplifier with a bandpass frequency from $1kHz$ to $500kHz$. Then the amplified signal is sent to the NI-7962R board, which runs at $4MHz$. The oscillation signal is processed by a $2nd$ order $330kHz - 370kHz$ bandpass filter to reduce unexpected noise. Then a $2nd$ order lowpass filter with a $100kHz$ cut-off frequency is applied to the absolute value of the bandpass filtered signal to achieve an averaging operation. The lowpass filtered signal is regarded as a measure of the oscillation amplitude and subsequently of the relative height.

The feedback loop is built in the NI LabVIEW real-time environment. The real-time digital feedback control is developed on an NI-7854R FPGA board, which is programmed to run at $500kHz$. The digital controller consists of a series of two digital filters. The relative height signal from the sensing functional component is sent to one input port of the NI-7854R through an Input/Output (I/O) terminal. This signal also in fact acts as the plant output. The reference signal is generated on-board using a digital signal generating program. The control signal calculated by the discrete transfer function goes through the I/O terminal to drive the fine piezo-actuator along the vertical direction.

III. PLANT ANALYSIS AND CONTROL DESIGN

In the vicinity of the range where the relative height sensing mechanism works, the cantilever is excited horizontally at $350kHz$, which is around one of the resonances in water. The appropriate cantilever excitation level is $0.04V$. This equates to a cantilever oscillating amplitude of $4nm$ outside the shear force interacting range (but within the evanescent field sensing range). The plant frequency response

is created by swept-sine system identification to measure the relative dynamics in vertical direction. The plant response remains constant with a gain of about $-25dB$ until $1kHz$. The frequency response has resonant peaks at approximately $35kHz$ with a gain of $-10dB$. Thus, the plant is modelled as a $6th$ order transfer function in continuous time as shown in Figure 2.

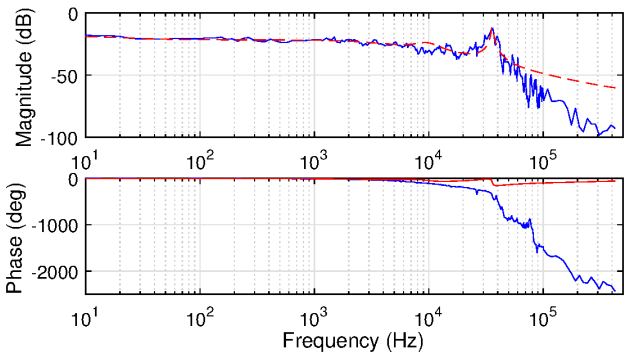

Fig. 2: Plant frequency response and fitted model of the vertically excited relative height plant.

Here a linear controller using a lag control concept is introduced to start with a constant gain at low frequency and end with a descending gain at high frequency. Two lags dropping their gain after $10Hz$ are designed to have sufficient low frequency gain and to avoid any significant control windup at low frequency. A notch filter is introduced to cancel the resonant peak at $35kHz$. A continuous time control is designed to perform an open loop response with a phase margin of $74.1°$ at the crossover frequency of $2.04kHz$ and a gain margin of over $25dB$.

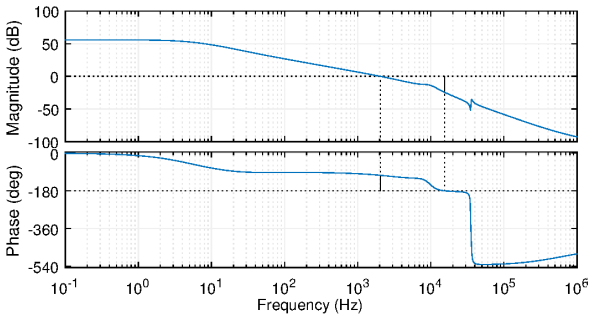

Fig. 3: Open-loop frequency response of the controlled plant, which is calculated from the fitted model and the designed controller in continuous time.

IV. FIXED-POINT-ARITHMETIC CONTROL DESIGN, SIMULATION, AND ANALYSIS

In AFM control, there are two solutions to the problem of implementation of the sensing and control algorithms with high bandwidth. One solution is to use specifically designed analogue circuits [8], and the other is to employ FPGAs running at very high clock frequencies ([14], [18], [16]). By implementing on FPGAs, the control development benefits from reliability, high-running-frequency, and obviously better prototyping-convenience than with analogue circuits. However, the FPGA based digital control implementation maybe unable to intuitively execute the designed digital-control program due to circuit design limitations and the nature of the binary numeric presentation in FPGAs. Moreover, FPGAs may require hours to compile and burn digital feedback control programs before validating the program for execution. Thus, it is important to verify FPGA control programs before loading and implementing on FPGA boards. Hence, the process will be to design at first continuous-time filters (or a controller) which is then discretized. Subsequently, a simulation based optimization of the FPGA-implementation parameters is practically carried out.

Practically, the commercial method to implement high order transfer functions is to employ loops for the repetitive fixed-point-arithmetic parts in a transfer function (see Discrete Transfer Function, Virtual Instrument (VI), from NI LabVIEW 2012 FPGA Module, www.ni.com). However, these loops have to run at a slower sampling frequency to obtain the filtering results. In practice, the loop design of a $6th$ order digital filter saves over 60% of the fixed-point arithmetic operations when compared to a transposed direct-form implementation. However, the direct form implementation permits the program to execute at a higher sampling rate than the NI-suggested loop-format program.

This paper suggests employing a bank of digital filters in series with a pre-chosen constant fixed-point-arithmetic range instead of verifying each arithmetic element carefully, since the amount of validation tests exponentially increases with respect to the order of the filter. For each filter component, a specific relative fixed-point value representation is used to avoid overflow and to improve calculation accuracy, and extra gains (realized by bit-shifts) are introduced before, between, and after each digital filter in the filter bank. The new 'internal' gains have to have an overall product of unity to retain the originally designed linear control performance. This permits better exploitation of the computational range of the digital filters, which are configured to have a specific fixed point representation.

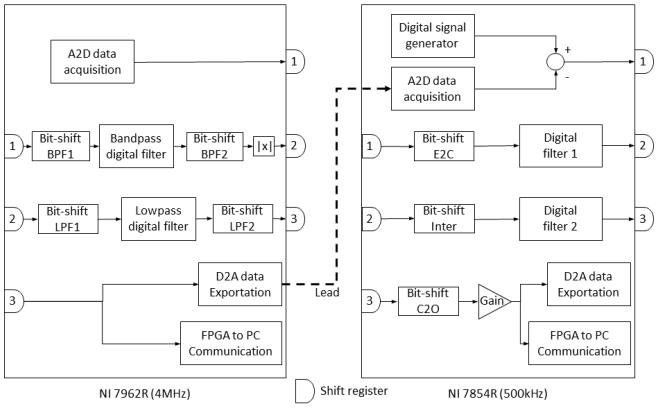

Fig. 4: Practical fixed-point-arithmetic based feedback control program layout on FPGA boards. To realize parallel programming, shift register can load the saved value from the previous running cycle.

The fixed-point-arithmetic based digital control is structured as in Figure 4. FPGA boards take a long time to execute analog-to-digital(A2D) conversion and digital-to-

analog (D2A) conversion. Thus, the data importation and exportation functions are designed to run as separate parallel programs. On the NI-7962R, two pairs of bit-shifts are associated with the bandpass filter and the lowpass filter. In each pair of bit-shifts, the first two operations $B^{>>}_{BPF1}$ and $B^{>>}_{LPF1}$ create bit-shifts on the input for the digital filter and the other two $B^{>>}_{BPF2}$ and $B^{>>}_{LPF2}$ perform an inverse bit-shift to rescale the output. Both the bandpass filter and the lowpass filter are implemented in controllable canonical form in a parallel manner to ensure running at a $4MHz$ clock frequency. Hence, the bandpass filter and lowpass filter (in discrete time) are given as

$$\begin{aligned} T_{BP}(z) &= \frac{0.005543z^2 + 0.01109z + 0.005543}{z^2 - 1.779z + 0.8008} \\ T_{LP}(z) &= \frac{0.03047z^2 - 0.03047}{z^2 - 1.654z + 0.9391} \end{aligned} \tag{1}$$

The feedback controller on the NI-7854R is realized at a $500kHz$ sampling frequency, which allows the running of the designed controller as two digital-filters in parallel. The Bit-shifts $B^{>>}_{E2C}$ and $B^{>>}_{Inter}$ are used to adjust the inputs to the digital filters to avoid overflow. Bit-shift $B^{>>}_{C2O}$ scales the output of the controller against the other two bit-shifts, in order to achieve overall unity gain. The scalar k_{Gain} is designed to further distribute the gain of the controller to reduce the chance of overflow in the two digital filtering programs. The feedback loop is constructed by calculating the error between the generated reference signal and the measured relative height signal. The fixed design of the two filters, F_1 and F_2, result from discretization at a $500kHz$ sampling frequency based on the lag controller also including an extra gain $k_{Gain} = 4$:

$$\begin{aligned} F_1(z) &= \frac{0.02703z - 0.02603}{z^2 - 1.951z + 0.9509} \\ F_2(z) &= \frac{0.8173z^2 - 1.479z + 0.8173}{z^2 - 1.479z + 0.6346} \end{aligned} \tag{2}$$

It is evident that the design of the bit-shift operators has to be systematically done off-line, as a change of the bit-shift operator characteristics can easily affect closed-loop stability (see fixed-point arithmetic simulation examples in Figure 5.(c)). Thus, a fixed-point arithmetic simulation scheme is proposed in this paper to resolve such issues before practical implementation. The tool is programmed in the Simulink (The MathWorks, Inc. (2017)) environment. Fixed-point-arithmetic operations are programmed using the fixed-point toolbox and respective time-delay elements. Hence, the NI-FPGA programs are simulated in discrete time with a fixed-point algorithm, identical to the FPGA settings. The identified plant model is simulated in continuous time.

The relative height sensing functional FPGA program is tested using different bit-shift pairs for $B^{>>}_{BPF1}$&$B^{>>}_{BPF2}$ and $B^{>>}_{LPF1}$&$B^{>>}_{LPF2}$ on the NI-7962R. The detected cantilever oscillation signal is given as a sine wave with an extreme amplitude of $2V$ at $350kHz$. Thus, the amplitude of the on-board measurement is converted into the maximum, $2^{15} - 1$, signed 16-bit integer. The bit-shifts $B^{>>}_{BPF1}$ and $B^{>>}_{LPF1}$ are tested from -32 bits to 32 bits with a step-size of 1-bit.

The criterion for testing the appropriateness of the fixed-point arithmetic sensing mechanism is to compare the sensing mechanism to the continuous-time simulation (as simulated for the NI-7962R). Thus, for comparison, the bandpass, the absolute value computation and the lowpass components are also simulated as continuous-time operators, while the output of these combined operations are sampled at $4MHz$ to give $s_{cnt}(k)$. The averaged absolute error $|\bar{E_S}|$ between the fixed-point-arithmetic simulation output, s_{fpga}, and the continuous-time simulation output, $s_{cnt}(k)$, gives the comparative measure:

$$|\bar{E_S}|_{(B^{>>}_{BP1}, B^{>>}_{LPF1})} = \frac{\sum_{k=0}^{m} |s_{fpga}(k) - s_{cnt}(k)|}{m} \tag{3}$$

where $s_{fpga}(k)$ is the relative height from the fixed-point-arithmetic simulation at the k-th sample time. The test simulation, for each parameter set, is run for $0.1s$ of simulation time, changing the amplitude of the input oscillation from $0V$ to $2V$. The averaged absolute error $|\bar{E_S}|_{(B^{>>}_{BP1}, B^{>>}_{LPF1})}$ as a function of the bit-shift values $B^{>>}_{BP1}$ and $B^{>>}_{LPF1}$ is in Figure 5.(a). The bit-shift operations clearly influence the performance of the proposed sensing mechanism.

For the feedback control program on the NI-7854R, the parametric configurations are tested for different bit-shift triples of $B^{>>}_{E2C}$, $B^{>>}_{Inter}$ and $B^{>>}_{C2O}$ from -32 to 32 bits. In fact, in this case, there is only freedom to optimize for bit-shifts $B^{>>}_{E2C}$ and $B^{>>}_{Inter}$, because bit-shift $B^{>>}_{C2O}$ has to realize the inverse of the other two operations to guarantee the overall gain of 1. For each bit-shift pair $B^{>>}_{E2C}$ and $B^{>>}_{Inter}$ of different configurations, the control reference (on-board) is given as a square wave at $10Hz$ with different amplitude levels for verifying the maximum controllable range. Specifically the amplitudes, r_{amp}, are configured as positive integers of 16 bits from 250 to 12500 which are kept constant during each simulation assessment. However, several tests are created, increasing at each simulation run the amplitude by 250. This creates a physical testing range of $0.76V$-$3.815V$ for this simulation. It will be seen that not every demand is feasible for this implementation, even after optimization of bit-shifts $B^{>>}_{E2C}$ and $B^{>>}_{Inter}$.

As a measure of assessment, the absolute value of the closed-loop control error, in a 16-bit integer representation, is exploited. Given a reference, $r(k)$, with an amplitude of r_{amp}, the evaluation $|\bar{E_C}|$ for a given bit-shift configuration of $B^{>>}_{E2C}$ and $B^{>>}_{Inter}$ is calculated as:

$$|\bar{E_C}|_{(B^{>>}_{E2C}, B^{>>}_{Inter}), r_{amp}} = \frac{\sum_{k=0}^{n} |r(k) - y(k)|}{n} \tag{4}$$

Here $r(k)$ and $y(k)$ are integer numbers representing the reference and plant output in closed-loop at the k-th simulated sampled-time. n is the maximum sampled simulation step run at $500kHz$ during the simulation time of $1s$. With the specific reference amplitude configuration of r_{amp}, the minimal $|\bar{E_C}|$ among all possible pairs of $(B^{>>}_{E2C}, B^{>>}_{Inter})$ setups is divided by r_{amp} to create the following ratio:

$$c_{E_C, r_{amp}} = \frac{\min_{(B^{>>}_{E2C}, B^{>>}_{Inter})} |\bar{E_C}|(B^{>>}_{E2C}, B^{>>}_{Inter}, r_{amp})}{r_{amp}} \tag{5}$$

The c_{E_C} for increasing r_{amp} in each optimization run is presented in Figure 5.(d) (Note the ordinate is scaled in $\%$

rather than within the range $[0, 1]$.) It is clear that the control error increases significantly when the reference amplitude is over 1000. With r_{amp} as 1000, the minimal c_{E_C} is less than 3% which indicates good feedback control performance of the fixed-point-arithmetic simulations. Moreover, $|\bar{E_C}|$ is shown in Figure 5.(b) while the feedback control reference amplitude is 1000. Three example configurations are picked and their simulations are shown in Figure 5.(c). Two of them are not feasible and unstable, i.e. $(B^{>>}_{E2c}, B^{>>}_{Inter}) = (-13, 15)$ and $(B^{>>}_{E2c}, B^{>>}_{Inter}) = (-13, -12)$. Hence, the evaluation figure indicates that the overflows happen in the two bright regions, which have to be avoided in any practical feedback control implementation. This is also to protect the practical equipment, such as the cantilever, from damage.

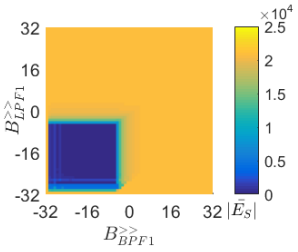

(a) Evaluation ($|\bar{E_s}|$) for sensing mechanism configuration on NI-7962R

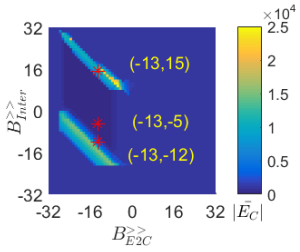

(b) Evaluation ($|\bar{E_c}|$) for feedback control configuration given $10Hz$ square wave reference amplitude as 1000 on NI-7854R

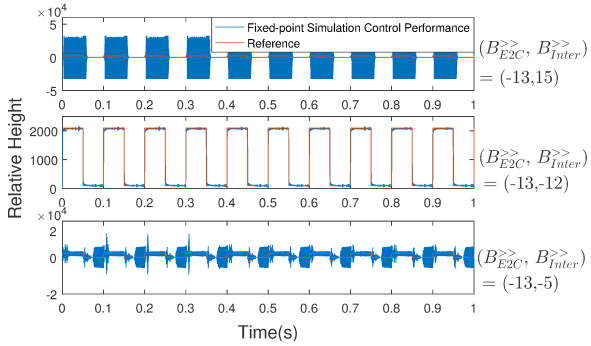

(c) Three fixed-point-arithmetic feedback control simulations for $10Hz$ square wave reference with different bit-shift operation configurations as marked in subfigure (b). Only $(B^{>>}_{E2c}, B^{>>}_{Inter}) = (-13, -5)$ permits a stable controller

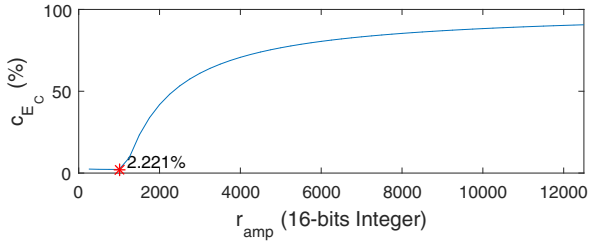

(d) Evaluation of feedback control configuration given $10Hz$ square wave reference with different amplitude on NI-7854R

Fig. 5: Evaluation of possible fixed-point-based FPGA programming configurations.

V. PRACTICAL PERFORMANCE AND NON-CONTACT SCAN RESULTS

This work has chosen the following FPGA program configurations based on guidance from the fixed-point-arithmetic simulations. The sensing functional filters both have an input bit-shift of -6 and an output bit-shift of 6. The $B^{>>}_{E2C}$, $B^{>>}_{Inter}$, and $B^{>>}_{C2O}$ are chosen as -19, 9, and 10. The cantilever is excited by a constant sine wave with an amplitude of $0.04V$ at $350kHz$. In a wet environment, the excitation drives the cantilever to create a sinusoidal response of approximately $4nm$ amplitude outside the shear-force interacting range. The strength of the evanescent field was carefully tuned to ensure an acceptable sensitivity to the cantilever motion. An offset along the vertical direction is imposed by the coarse piezo-actuator to place the cantilever into the shear-force interacting range for cantilever oscillation detection (see Figure 6). The vertical-axis control relies on the fine piezo-actuator with high actuation precision at $22nm/V$. Consequently, the vertical control which is developed and implemented to track different given relative height references, i.e. the relative height based control can track the sample-substrate profile in non-contact mode.

A. Nonlinear Plant Characteristics

The nonlinearity of the proposed sensing mechanism was initially measured by recording the measured relative height value (represented as a signed 16-bit integer number on the NI-7854R board) and the distance (deducted according to the travelling distance of piezo-actuation) from the cantilever to the sample-substrate. The measurement (see Figure 6) is collected by lifting up the relative height from $0nm$ to $25nm$, which approximately equals the relative height value from 0 to 800 during the experiment, without vertical closed-loop control. Outside this region, i.e. above $25nm$, this amplitude measure becomes non-monotonic in these conditions. Hence, the ordered water layer defines the range of relative measurement. It is obvious that the plant has strong nonlinear characteristics at different relative height levels. Consequently the feedback control performance (see examples in Figure 7) is significantly influenced by the nonlinearity.

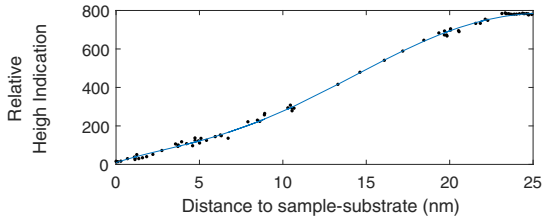

Fig. 6: Nonlinearity of the proposed sensing mechanism employing amplitude detection.

B. Control Characteristics

The control performance is investigated to prepare for non-contact mode scanning of the TDFM. As in the previous system identification test, the control performance is tested at 100 and 400 relative height indication levels. The tracking reference signals are both square wave signals with an amplitude of 50 relative height. To ensure sufficient settling time in each case, the reference square signals have a frequency of $50Hz$ and $100Hz$ at 100 and 400 relative height levels respectively (see Figure 7).

The digital control implementation is capable of tracking rapidly the changing sample-substrate height in a liquid environment. The closed-loop system has a settling time of

about $0.3ms$ at a relative height level of 400 and of about $0.8ms$ at a relative height level of 100. As a result, the closed-loop bandwidth is about $3kHz$ and $1.2kHz$ at the two relative height levels.

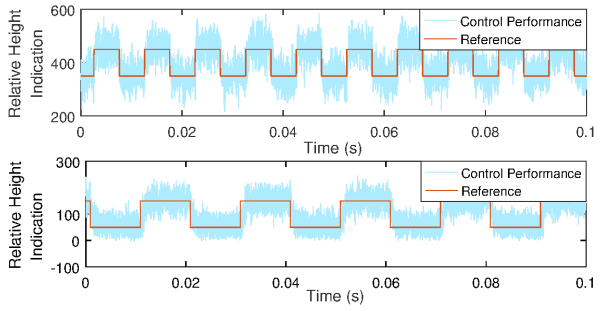

Fig. 7: Closed-loop reference tracking control performance at different relative height levels.

C. Scanning Result

The overall target of the control design is to realize a non-contact mode scan. Moreover, a successful scan verifies that the proposed shear force interaction sensing scheme is suitable for relative height detection and scanning. To conduct non-contact mode scans, the relative height control is complemented with a horizontal x-y stage $P.734.CL$ (PI). The x-y in-plane motion is realized with a control amplifier box E-710 (PI). The x-y motion signal is generated from a digital trajectory planning program on the NI-7854R, which produces a customisable raster motion. The x-axis presents the fast scanning direction and the y-axis the slow scanning direction.

The scanned samples considered in this paper are simple with constant regular shapes to verify non-contact scanning in pure water. Plastic sphere particles ([19]) approximately $50nm$ in diameter are attached to a glass slide by a $NiCl_2$ solution, acting as an adhesive between the spheres and the slide. The scanned sample-substrate topography is calibrated by the absolute height measurement (Figure 8).

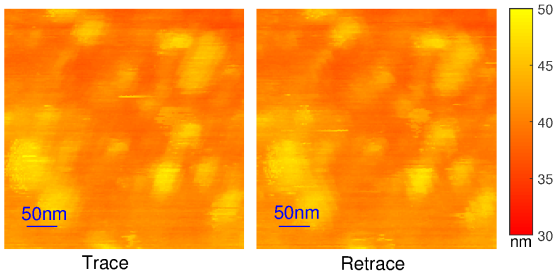

Fig. 8: TDFM non-contact mode scan of 50nm sphere particles with a $1Hz$ raster scanning rate in water. The scanned area is 400nm $\times$400nm with 150×150 pixels resolution.

The imaged particles have sphere shapes of about $50nm$ diameter in all three directions, i.e. the developed relative height control has provided an accurate topography measurement at nano-scale.

VI. CONCLUSIONS

This paper has described an FPGA based digital control design employing a relative height sensing mechanism for the TDFM system, which is unique to other SFM techniques. To realize non-contact mode scans in a wet environment, the plant model was identified in open-loop and a single-input-single-output controller was designed. A fixed-point-arithmetic digital control implementation is suggested for the FPGA system taking into account practical signal limits and addressing overflow issues. To achieve this, an optimization based on a fixed-point-arithmetic simulation scheme was carried out. It provides an efficient and sound method for prior-testing of FPGA based digital control implementations. Practical results show the nonlinear characteristics of the controlled plant, which probably necessitates a more advanced controller design in the future. Nevertheless, this paper presents the very first complete relative height control based imaging results of nano-particles from the TDFM system, and shows the potential of the TDFM device for non-contact mode scanning.

REFERENCES

[1] E. Betzig, P. Finn, and J. Weiner, "Combined shear force and near-field scanning optical microscopy," *Appl. Phys. Lett.*, 1992.

[2] M. Antognozzi, A. Ulcinas, L. Picco, S. Simpson, P. Heard, M. Szczelkun, B. Brenner, and M. Miles, "A new detection system for extremely small vertically mounted cantilevers," *Nanotechn.*, 2008.

[3] M. Antognozzi, M. D. Szczelkun, A. N. Round, and M. J. Miles, "Comparison between shear force and tapping mode afm-high resolution imaging of DNA," *Single Molecules*, 2002.

[4] J. M. Fletcher, R. L. Harniman, F. R. Barnes, A. L. Boyle, A. Collins, J. Mantell, T. H. Sharp, M. Antognozzi, *et al.*, "Self-assembling cages from coiled-coil peptide modules," *Science*, 2013.

[5] P. Sandoz, J.-M. Friedt, and E. Carry, "Vibration amplitude of a tip-loaded quartz tuning fork during shear force microscopy scanning," *Rev. Sci. Instrum.*, 2008.

[6] A. La Rosa, X. Cui, J. McCollum, N. Li, and R. Nordstrom, "The ultrasonic/shear-force microscope: Integrating ultrasonic sensing into a near-field scanning optical microscope," *Rev. Sci. Instrum.*, 2005.

[7] K. Karrai and I. Tiemann, "Interfacial shear force microscopy," *Phys. Rev. B*, 2000.

[8] T. Ando, "High-speed AFM imaging," *Current opinion in structural biology*, 2014.

[9] G. Binnig, C. F. Quate, and C. Gerber, "Atomic force microscope," *Phys. Rev. Lett.*, 1986.

[10] A. Sikora, T. Gotszalk, A. Sankowska, and I. W. Rangelow, "Application of scanning shear-force microscope for fabrication of nanostructures," *Jrnl. of Telecom. and Info. Technol.*, 2005.

[11] M. Koopman, B. De Bakker, M. Garcia-Parajo, and N. Van Hulst, "Shear force imaging of soft samples in liquid using a diving bell concept," *Appl. Phys. Lett.*, 2003.

[12] T. Hatano, K. Zhang, S. Khan, T. Nguyen, G. Herrmann, C. Edwards, S. Burgess, and M. Miles, "A specimen-tracking controller for the transverse dynamic force microscope in non-contact mode," in *ACC*, 2016.

[13] M. Antognozzi, A. Protti, M. Miles, and G. Valdr, "Investigation of nano-confined liquids on muscovite by transverse dynamic force microscopy (TDFM)," *GeoActa*. Publisher: University of Bologna.

[14] I. Soltani Bozchalooi, *Design and control of high-speed and large-range atomic force microscope*. PhD thesis, Massachusetts Institute of Technology, 2015.

[15] S. Kuiper, P. Van den Hof, and G. Schitter, "Integrated design of the feedback controller and topography estimator for atomic force microscopy," *Control Eng Pract.*, 2013.

[16] J. L. Jerez, P. J. Goulart, S. Richter, G. A. Constantinides, E. C. Kerrigan, and M. Morari, "Embedded predictive control on an FPGA using the fast gradient method," in *ECC*, 2013.

[17] G. Schitter and N. Phan, "Field programmable analog array (FPAA) based control of an atomic force microscope," in *ACC*, 2008.

[18] P. Huang, *Algorithmic approaches to high speed atomic force microscopy*. PhD thesis, Boston University, 2013.

[19] T. F. S. Inc., "Thermo scientific particle technology product catalog and technical reference guide," 2011.